Colloidal Silica Films for High-Capacity DNA Probe Arrays

M. Glazer,*,†,‡ J. Fidanza,§ G. McGall,§ and C. Frank‡

Departments of Chemical Engineering and Materials Science and Engineering, Stanford University, Stanford, California 94305, and Affymetrix, Santa Clara, California 95051

Received June 25, 2001

The use of arrays of immobilized DNA "probes" for high-throughput analysis of genomic samples is expanding rapidly. The detection sensitivity of these arrays depends on the quantity and density of immobilized probe molecules as well as on the thermodynamics and kinetics of nucleic acid hybridization. We have prepared and investigated substrates with a porous, "three-dimensional" surface layer as a means of increasing the surface area available for the synthesis or immobilization of oligonucleotide probes, thereby increasing the number of available probes and the amount of detectable bound target per unit area. Surfaces with pores 5 nm and larger were created by spin-coating colloidal suspensions of silica particles, followed by thermal curing. DNA arrays were synthesized on the resulting surfaces by photolithographic patterning, and the performance on the high-capacity substrates was compared to that on standard flat glass surfaces. The colloidal silica films created via this route show equivalent performance to flat glass substrates in terms of the efficiency of chemical synthesis and resolution of photolithographic patterning. DNA targets are able to penetrate the porous layers, and under saturating conditions, the quantity of bound target is proportional to the layer thickness. The result is an enhanced hybridization signal that is 20 times higher than flat glass for a colloidal particle layer that is 0.5 μm thick. The thermodynamic stability of probe/target duplexes in the matrix is the same as that for their counterparts on flat surfaces, although the colloidal silica films reach saturation more slowly than flat surfaces.

Introduction

Recent initiatives to obtain complete genomic sequences for humans and other organisms have increased the demand for techniques that enable the rapid, large-scale analysis of DNA and RNA. Hybridization-based sequence analysis using high-density polynucleotide probe arrays is capable of efficiently accessing large amounts of genetic information from biological samples in a single assay procedure.[1,2] These arrays, or "DNA chips," are essentially large sets of nucleic acid "probe" sequences that are immobilized in defined locations on the surface of a flat substrate, typically glass. Light-directed combinatorial synthesis has enabled the fabrication of oligonucleotide probe arrays with very high resolution and information content on a commercial scale.[3,4] In a typical application, DNA or RNA "target" sequences of interest are isolated from a biological sample using standard molecular biology protocols.[5] The analyte sequences are fragmented and labeled with reporter molecules (such as fluorescent labels) for detection, and the mixture of labeled fragments is applied to the array under controlled conditions, allowing binding to surface probes that have complementary sequences (hybridization). The array is then imaged, typically with a laser confocal scanning microscopy system, to locate and quantify the binding of target sequences from the sample to complementary sequences on the array. Application-specific software reconstructs and presents the sequence data for further querying.

The ability to detect the binding of target molecules from a nucleic acid sample to complementary probes on an array depends on a large number of factors, including the quantity and density of immobilized probe molecules on the substrate.[6] A variety of methods have been used to increase the number of probe molecules available for binding and thereby increase the sensitivity of DNA arrays. Much of the focus has been on organic surface modification, including polymer gel layers,[7−9] organic

* To whom correspondence should be addressed. E-mail: mglazer@leland.stanford.edu.

† Department of Materials Science and Engineering, Stanford University.

‡ Department of Chemical Engineering, Stanford University.

§ Affymetrix.

(1) Lockhart, D. J.; Dong, H.; Byrne, M. C.; Follettie, M. T.; Gallo, M. V.; Chee, M. S.; Mittman,M.; Wang, C.; Kobayashi, M.; Horton, H.; Brown, E. L. *Nat. Biotechnol.* **1996**, *14*, 1675−1680.

(2) Lipshutz, R. J.; Morris, D.; Chee, M.; Hubbell, E.; Kozal, M. J.; Shah, N.; Shen, N.; Yang, R.; Fodor, S. P. A. *BioTechniques* **1995**, *19*, 442−447.

(3) Fodor, S. P. A.; Read, J. L.; Pirrung, M. C.; Stryer, L.; Lu, A. T.; Solad, D. *Science* **1991**, *251*, 767−773.

(4) Pease, A. C.; Solas, D.; Sullivan, E.; Cronin, M. T.; Holmes, C. P.; Fodor, S. P. A. *PNAS* **1994**, *91*, 5022−5026.

(5) Schena, M.; Davis, R. W. In *Microarray Biochip Technology*; Schena, M., Ed.; Eaton Publishing: Natwick, MA, 2000; p 1.

(6) Steel, A.; Torres, M.; Hartwell, J.; Yu, Y.; Ting, N.; Hoke, G.; Yang, H. In *Microarray Biochip Technology*; Schena, M., Ed.; Eaton Publishing: Natwick, MA, 2000; pp 87−117.

(7) Heller, M. J.; Forester, A. H.; Tu, E. *Electrophoresis* **2000**, *21*, 157−164.

10.1021/cm010578n CCC: $20.00
Published on Web 11/30/2001

membranes,[10,11] and dendrimeric linking molecules.[12] However, these approaches present certain drawbacks. For instance, the kinetics of diffusion of the target nucleic acid molecules in a polymer gel will be slower than that in solution due to the higher viscosity of the gel and also due to nonspecific interactions with the immobilized nucleic acid probes and potentially with the matrix itself.[13] DNA dendrimers have also been utilized to increase the number of sites available for binding target molecules, but the sensitivity gains with this approach are lower than expected, suggesting that many of the binding sites may be inaccessible due to steric crowding.[14]

Porous inorganic substrates are receiving increasing attention as potential supports for DNA arrays. Inorganic materials are inert to most processes used for array fabrication and testing, which is one of the reasons for the widespread use of flat glass substrates. Previously, oligonucleotides or DNA fragments have been immobilized on alumina filters,[10] porous silicon,[15] and "flow-through" chips consisting of glass capillaries.[6] However, due to optical scattering that would result from the large features and opaqueness (in the case of silicon), these materials are not well-suited to high-resolution photolithographic array synthesis. Furthermore, since confocal microscopy is extremely sensitive to scattered light,[16] scattering from large features in the film adversely affects the resolution of the imaging system.

Photolithographic patterning enables the synthesis of DNA arrays with very small feature sizes, and thus extremely high information content can be obtained. This process involves the selective removal of terminal-protecting groups from growing oligonucleotide chains in predefined regions of a glass support by controlled exposure to light through photolithographic masks.[3,4] Oligonucleotide building blocks with photolabile 5′-protecting groups are added to the growing probes in a step-by-step process. For photolithography, the pore size of the features must be substantially smaller than the wavelength of light to avoid optical scattering. We have recently reported preliminary results using colloidal silica films as substrates for photolithographically patterned arrays.[17,18] Deposition of colloidal silica as a route for creating porous thin films has several favorable characteristics. For example, dip and spin-coating techniques for the deposition of colloidal films have been well established.[19] Furthermore, the use of rigid colloidal silica particles rather than molecular precursors (such as alkoxides) gives mechanical strength to the porous layers with minimal sintering. Additionally, the use of rigid precursors makes the deposition process more robust and less sensitive to the environment (humidity, temperature) and stoichiometry parameters that are critical conditions for control of the hydrolysis and condensation reactions that occur during the spin-coating of alkoxides.[19] Finally, the size of the precursors can be chosen to create the appropriate pore size to accommodate different target molecules, with the porosity being independent of the particle size (for relatively monodisperse particles). To further control and optimize the morphology of these types of films, latex particles can be incorporated during the film deposition process and then removed at high temperatures, leaving behind voids of a controlled size.[18] Pore sizes less than 30 nm can be readily obtained, resulting in films with extremely high surface area.

In this work, we present detailed characterization of colloidal silica films relevant to their use as substrates for high-capacity DNA arrays and we discuss colloidal silica film deposition, chemical synthesis of arrays, optical imaging, and the hybridization of oligonucleotide target molecules. The use of oligonucleotide targets in this study eliminates concerns about nonspecific binding of background cell material present in biological samples so that fundamental differences in thermodynamic and kinetic behavior of probe/target binding in the matrix can be observed.

This study has been conducted simultaneously with the evaluation of colloidal silica substrates in complex, high-density biological assays such as those used for disease management and Human Gene Expression profiling. Using colloidal silica films, we have demonstrated an 8 to 10-fold improvement in signals and a higher percentage of correct calls of the target sequence in an assay for the protease and reverse transcriptase genes of the HIV virus.[20] The performance of Human Gene Expression profiling arrays using these substrates will be discussed in a separate report.[21]

Experimental Procedures

Film Deposition. Testing was performed on soda-lime (Erie Scientific) and fused silica (U.S. Precision Glass) glass substrates. Test pieces were cut to either $2 \times 3 \times 0.027$ in. or $5 \times 5 \times 0.027$ in. All substrates were cleaned via a three-step process of soaking in Nanostrip (sulfuric acid and hydrogen peroxide, Cyantek, 15 min), sodium hydroxide solution (10% by wt in water, 70 °C, 3 min), and hydrochloric acid (0.4% by wt in water, 1 min).

Film deposition was accomplished via spin-coating of colloidal silica suspensions. The silica solutions used were Snowtex S50, 20L, and ZL (Nissan Chemicals), which were analyzed prior to deposition by dynamic light scattering (DLS) with laser wavelength of 514.5 nm (Brookhaven Instruments) to observe the actual size distribution of the particles. The measured sizes of the S50, 20L, and ZL particles were 16 ± 5, 54 ± 13, and 65 ± 16 nm, respectively.

(8) Proudnikov, D.; Timofeev, E.; Mirzabekov, A. *Anal. Biochem.* **1998**, *259*, 34.
(9) Yershov, G.; Barsky, V.; Belgovskiy, A.; Kirillov, E.; Dreindlin, E.; Ivanov, I.; Parinov, S.; Guschin, D.; Drobishev, A.; Dubiley, S.; Mirzabekov, A. *PNAS* **1996**, *93*, 4913−4918.
(10) Englert, D. In *Microarray Biochip Technology*; Schena, M., Ed.; Eaton Publishing: Natwick, MA, 2000; pp 220−240.
(11) Matysiak, S.; Hauser, N. C.; Wurtz, S.; Hoheisel, J. D. *Nucleosides Nucleotides* **1999**, *18*, 1289.
(12) Beier, M.; Hoheisel, J. D. *Nucleic Acids Res.* **1999**, *27*, 1970.
(13) Livshits, M. A.; Mirzabekov, A. *Biophys. J.* **1996**, *71*, 2795.
(14) Wang, J.; Miang, M.; Nilsen, T. W.; Getts, R. C. *J. Am. Chem. Soc.* **1998**, *120*, 8281−8282.
(15) Lin, V. S.-Y.; Motesharei, K.; Dancil, K.-P. S.; Sailor, M. J.; Ghadiri, M. R. *Science* **1997**, *278*, 840.
(16) Schermer, M. J. In *DNA Microarrays*; Schena, M., Ed.; Oxford Press: New York, 1999; pp 17−42.
(17) Glazer, M.; Frank, C.; Vinci, R. P.; McGall, G.; Fidanza, J.; Beecher, J. In *Organic/Inorganic Hybrid Materials II*; Klein, L, C., Francais, L. F., DeGuire, M. R., Mark, J. E., Eds.; Materials Research Society Proceedings: PA, 1999; pp 371−376.
(18) Glazer, M.; Frank, C.; Lussi, J.; Fidanza, J.; McGall, G. In *Organic/Inorganic Hybrid Materials−2000*; Laine, R. M., Sanchez, C., Brinker, C. J., Giannelis, E., Eds.; Materials Research Society Proceedings, 2001; pp CC10.4.1−CC10.4.6 (online publication).
(19) Brinker, C. J.; Scherer, G. W. *Sol−Gel Science*; Academic Press: San Diego, 1990; pp 787−797.
(20) Fidanza, J.; Glazer, M.; Mutnick, D.; McGall, G.; Frank, C. *Nucleosides Nucleotides* **2001**, *20*, 533−538.
(21) Fidanza, J.; Glazer, M.; Frank, C.; McGall, G. In preparation.

The suspensions were diluted to the desired weight concentration with deionized water, dispensed onto the glass substrates using a syringe with a 0.45 μm filter, and then spun at 2500 rpm for 30 s. Drying typically occurred in 15−20 s, as could be observed by the color change of silicon substrates spun under the same conditions. The films were then heated at a rate of 10 °C min^{-1} and held at 350 °C for 4 h. This temperature was sufficient to provide stable films (see Results) while avoiding excessive sintering that could change the film morphology and cause shrinkage if elevated temperatures were used.

Nitrogen Adsorption. To obtain samples of sufficient size for the measurement of surface area, pore size, and pore volume, colloidal silica suspensions were dried in an oven at 80 °C for 12 h and then at 100 °C for 6 h, and samples of the dried materials were analyzed with a Beckman−Coulter SA-3100. Samples were outgassed at 300 °C for 60 min, and nitrogen was used as the adsorbate gas. The Brunauer, Emmett, and Teller (BET) method was used for calculating surface area, and the Barret, Joyner, and Halenda (BJH) method was used for calculating pore volume and size distribution.[22]

Film Characterization. Ellipsometric measurements were conducted on films deposited on silicon, which provides a higher contrast in the index of refraction than glass, with the native oxide surface layer on the silicon providing a substrate similar to the glass surface. Measurements were made with a Gaertner ellipsometer at a wavelength of 632.8 nm. Film thickness measurements were made with a Dektak 3 surface profilometer (Veeco).

Electron microscopy measurements were made on a Hitachi S4700 field emission scanning electron microscope. A thin layer of gold was sputtered onto the surface before imaging the glass.

Surface area of the deposited films is calculated by combining results from ellipsometry and nitrogen adsorption. From measurements of the index of refraction, the mass of the solid phase (M_s) in the layer is calculated by eq 1, which is based on the Lorentz−Lorenz equation.[23,24]

$$M_s = \left(\frac{N_f^2 - 1}{N_f^2 + 2}\right)\left(\frac{N_{si}^2 + 2}{N_{si}^2 - 1}\right)t\rho_{si} \quad (\text{in g cm}^{-2}\text{ of lateral surface}) \tag{1}$$

N_f and N_{si} are the indices of refraction of the film and pure SiO_2 (1.46), respectively, t is the film thickness, and ρ_{si} is the density of pure SiO_2 (2.2 g cm^{-3}). The area factor (AF), which quantifies the multiple of surface area relative to a flat glass substrate for a given lateral area, is then calculated with eq 2.

$$AF = M_s A_N + 1 \tag{2}$$

A_N is the specific surface area (m^2 g^{-1}) of the dried colloidal material from nitrogen adsorption measurements, and the additional term of unity is included to account for the original flat surface on which the layer was deposited.

Chemical Coupling Efficiency. Prior to synthesis of oligonucleotide probes on the substrates, the surface was silanated with bis(2-hydroxyethyl)-3-aminopropyltriethoxysilane.[17,18] Two complementary techniques were then used to study the coupling of phosphoramidites to the resulting surface hydroxyl groups on the silane, which serve as initiation sites for oligonucleotide synthesis. The hydroxyl groups were labeled with a fluorescein phosphoramidite using standard phosphoramidite coupling protocols.[25] The amount of bound fluorescein was analyzed by directly imaging the fluorescence with a confocal system or by cleaving the fluorescein molecules from the surface and then quantifying the total amount of fluorescein molecules released using high-performance liquid chromatography (HPLC).

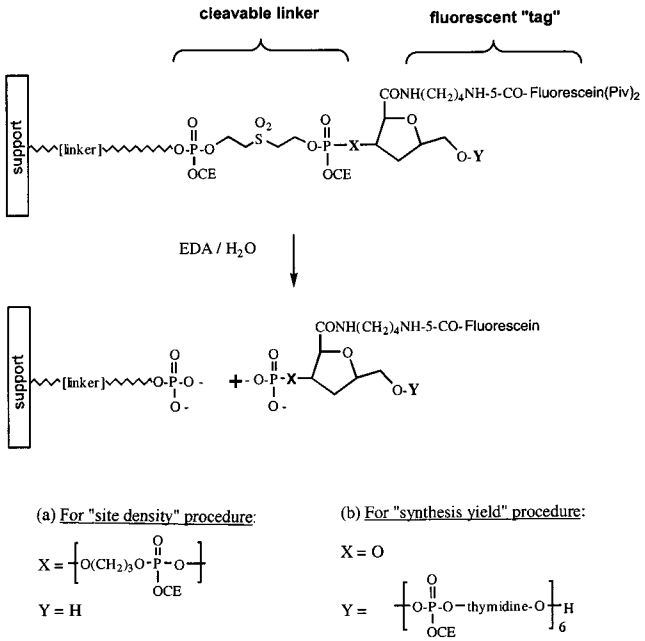

Figure 1. Procedures for quantification of (a) surface hydroxyl site density (pmol cm^{-2}) and (b) stepwise synthesis efficiency (RSY). The cleaved products are quantified by HPLC; CE = 2-cyanoethyl and Piv = pivaloyl.

Surface Fluorescence Analysis. Quantitative studies of the density and uniformity of chemical coupling on the substrates were conducted using "surface-staining" methods[25] in which a fluorescein phosphoramidite derivative is coupled to the free hydroxyl groups on the silane. Prior to staining, the fluorescein phosphoramidite monomer was diluted with the appropriate amount of a diluent monomer (T β-cyanoethyl phosphoramidite (DMT-T-CEP), Amersham Pharmacia) in acetonitrile to a total concentration of 50 mM. To deprotect the bound fluorescein molecules, the substrates were treated in a 1:1 solution of ethylenediamine/ethanol for 1 h, rinsed with deionized water, and dried with nitrogen. The substrates were then scanned with a confocal laser scanning microscope,[25] with the signal obtained being a function of the number of available sites on the surface. The signal was calibrated with solutions of fluorescein sodium salt (Sigma) in buffer to correlate values obtained with the actual surface density of fluorophores.

HPLC Analysis. A HPLC assay[26−28] was used to measure the hydroxyl site density available for synthesizing oligonucleotides, the synthesis efficiency on the support, and the extent of adsorption or entrapment of the reagents within the porous matrix (see Figure 1). For site density measurement, a cleavable linker (5′-phosphate-ON reagent, ChemGenes Corp.) was attached to the surface with phosphoramidite chemistry, followed by a spacer molecule (C_3 spacer phosphoramidite, Glen Research) and a fluorescent tag prepared separately (5′-carboxyfluorescein phosphoramidite[27]). The surface was then

(22) Allen, T. *Particle Size Measurement, Surface Area and Pore Size Determination*, 5th ed.; Chapman & Hall: London, 1997; Chapter 2.

(23) Pettit, R.; Ashley, C.; Reed, S.; Brinker, J. In *Sol−Gel Technology for Thin Films, Fibers, Preforms, Electronics, and Specialty Shapes*; Klein, L., Ed.; Noyes Publications: NJ, 1988; p 85.

(24) Born, M.; Wolf, E. *Principles of Optics*, 6th ed.; Pergamon Press: New York, 1980; pp 86−88.

(25) McGall, G. H.; Barone, A. D.; Diggelmann, M.; Fodor, S. P. A.; Gentalen, E.; Ngo, N. *J. Am. Chem. Soc.* **1997**, *119*, 5081−5090.

(26) U.S. Patent 5,843,655.

(27) Eur. Pat. Appl. EP 967217, 1999.

(28) McGall, G. H.; Barone, A. D.; Beecher, J. E.; Diggelman, M.; Fodor, S. P. A.; Goldberg, M. J.; Ngo, N.; Rava, R. P. In *Innovation and perspectives in solid phase synthesis and combinatorial libraries, 1998: peptides, proteins and nucleic acids: small molecule organic chemical diversity: collected papers, fifth international symposium*, 5th ed.; Epton, R., Ed.; Mayflower: London, 1999; pp 97−100.

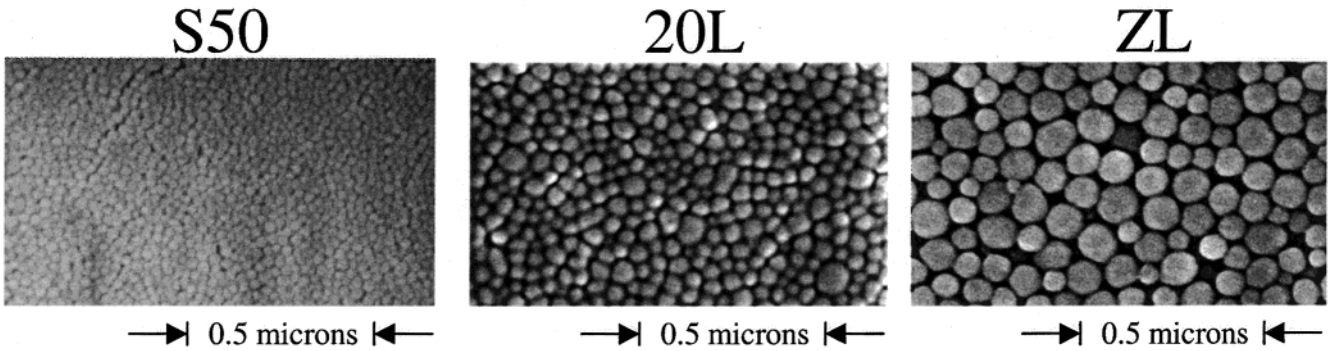

Figure 2. Scanning electron microscope (SEM) image of colloidal silica particles deposited on glass.

diced into 1 cm^2 pieces, weighed, placed in a glass vial, and treated with 1:1 (by vol) ethylenediamine/water for 4 h at 50 °C to cleave the linker and release $^{3'}pC_3$-fluorescein$^{5'}$. The resulting solution was diluted, co-injected with an internal standard, and analyzed by HPLC. The internal standard, $^{3'}pC_3C_3$-fluorescein$^{5'}$, was prepared separately on an ABI synthesizer and quantified independently by UV−Vis spectra on a Varian Cary 3E spectrophotometer (Varian).

HPLC analyses were performed on a Beckman System Gold employing an ion-exchange column and fluorescence detection at 520 nm. Elution was performed with a linear gradient of 0.4 M $NaClO_4$ in 20 mM Tris pH 8 (or other suitable buffer system), at a flow rate of 1 mL min^{-1}. If fluorescent molecules have remained adsorbed or trapped on the surface non-covalently, they will appear first in the chromatogram, followed by fluorescein that has coupled to the C_3 spacers and finally the $^{3'}pC_3C_3$-fluorescein$^{5'}$ internal standard. Integration of HPLC peak areas was used to quantify the total cleaved fluorescein and thereby the total site density. The surface site density per unit area was determined by dividing the total sites by the lateral surface area available for synthesis (calculated from the weight of the glass sample).

The efficiency of oligonucleotide synthesis was determined by examining the yield of a short homopolymer, such as hexathymidylate. The cleavable linker was coupled to the surface, followed by a fluorescein phosphoramidite and six nucleoside phosphoramidites (see Figure 1). The homopolymer was then cleaved from the support, mixed with an internal standard, and analyzed by HPLC. The relative synthesis yield (RSY) on the surface was calculated by dividing the integrated area of the 6-mer peak by the total area of all products cleaved from the surface. The RSY is indicative of the efficiency of the step-by-step base-coupling reactions on the solid support.

Hybridization to Oligonucleotide Targets. 20-mer probes were synthesized in a checkerboard pattern on Affymetrix photolithographic synthesizers using phosphoramidite chemistry, followed by removal of protecting groups in 1:1 (by vol) ethylenediamine/ethanol solutions for a minimum of 4 h.[25] A typical probe sequence used for analysis was (from surface) 3′-GACTTGCCATCGTAGAACTG-5′. The arrays were hybridized to solutions of 100 nM 5′-fluorescein-labeled oligonucleotide target in 0.1 M MES (2-[*N*-morpholino]ethanesulfonic acid (Sigma)) buffer (0.89 M NaCl, 0.03 M NaOH). A target concentration of 100 nM was used, as this concentration has previously been shown by Forman et al.[29] to saturate the surface probes in a similar system, resulting in the highest adsorbed target density. The films were scanned at several time points in 25 °C buffer (36 h) and then transferred to buffer maintained at 45 °C (50 h) with an environmental incubator shaker (New Brunswick Scientific). Prior to scanning, the samples were extensively washed with fresh buffer to remove nonspecifically bound target.

To evaluate discrimination, probes were synthesized with the perfect-match sequences, as well as with single-base mismatches at base 10 (A substituted for T) and two-base mismatches with substitutions at both base 10 and base 12 (A substituted for G).[29] Discrimination was evaluated by comparing the relative signal intensity (after background correction) in the mismatch regions with the signal in the perfect-match region.

Table 1. Parameters of Dried Colloidal Silica Measured by Nitrogen Adsorption

sample	mean particle size (nm)	BET surface area ($m^2\ g^{-1}$)	mean pore diameter (nm)	pore volume (mL g^{-1})
S50	16 ± 5	104	5.3 ± 0.2	0.19
20L	54 ± 13	49	14.2 ± 0.7	0.22
ZL	65 ± 16	35	22.5 ± 2.2	0.21

Results

Suspension and Film Characterization. Figure 2 shows SEM images of the S50, 20L, and ZL silica particles deposited on a glass surface (after 350 °C treatment). The particles pack randomly with no noticeable short- or long-range order. The broad distribution observed by light scattering is also reflected in the distribution of particle sizes in the deposited layer. The implications of the broad particle size distribution are considered in the Discussion. The index of refraction of the colloidal silica films was typically 1.3 before the 350 °C thermal treatment and did not increase following the treatment, indicating that the curing process did not cause significant densification of the films. Therefore, the properties of the dried material should be comparable to the structure following thermal treatment.

The pore size, surface area, and pore volume for bulk-dried colloidal silica are summarized in Table 1. Pores in this system are the void spaces between the solid particles. The smaller particle sizes have correspondingly smaller pores and higher surface area, whereas the total pore volume is nearly constant. The pores are considerably smaller than the pores in standard controlled pore glass (CPG) supports for DNA synthesis, which are typically 50−100 nm.[30]

Site Density and Coupling Yield. The surface-site-density procedure was used to evaluate the efficiency of phosphoramidite chemistry on the porous films. Analysis of the HPLC chromatograms for the cleaved products showed peaks corresponding only to the expected $^{3'}pC_3$-fluorescein$^{5'}$ and internal standard. The C_3 spacer serves as a control for incomplete coupling or removal of reagents from the porous matrix. If the

(29) Forman, J. E.; Walton, I. D.; Stern, D.; Rava, R. P.; Trulson, M. O. In *Molecular Modeling of Nucleic Acids*; Leonitis, N. B., SantaLucia, J., Jr., Eds.; ACS Symposium Series 682; American Chemical Society: Washington, DC, 1998; pp 206−228.

(30) Adams, S. P.; Kavka, K. S.; Wykes, E. J.; Holder, S. B.; Gallupi, G. R. *J. Am. Chem. Soc.* **1983**, *105*, 661.

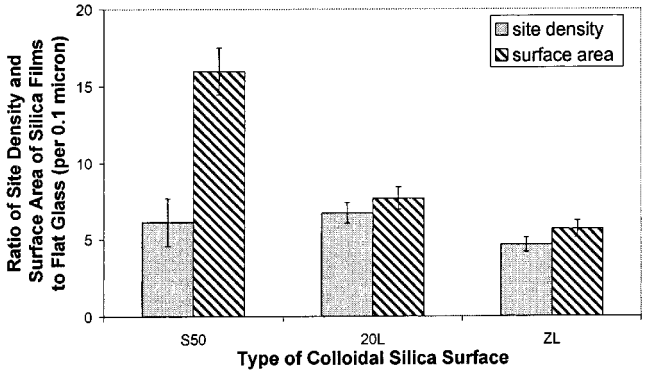

Figure 3. Comparison of the density of accessible surface hydroxyl sites to the surface area of the porous films. Reagents are able to fully access the 20L and ZL surfaces, but complete coupling is not achieved on the S50 surface due to poor fluid flow in the small pores.

Table 2. Synthesis Yield on Colloidal Silica Films[a]

particle type	relative synthesis yield (flat glass = 1)
S50	0.46 ± 0.44
20L	1.07 ± 0.09
ZL	1.11 ± 0.10

[a] Normalized to flat glass [= RSY_{film}/RSY_{flat}].

fluorescein reagents were not completely washed out of the matrix during coupling, a separate peak, corresponding to the fluorescein phosphate monomer, would elute prior to that for the $^{3'}pC_3$-fluorescein$^{5'}$. The fact that all of the fluorescein that eluted from the surface was covalently attached to C_3 spacers indicated that coupling was efficient in the porous film.

Figure 3 shows the quantification of the hydroxyl site density experiments for each of the particle types in comparison to the actual surface area of the film. Layers were deposited from 20 wt % suspensions, resulting in 0.3 μm films for all three particle types. Measured site density on the flat glass was 120 ± 10 pmol cm^{-2}. For the 20L and ZL films, the increase in site density agrees with that predicted by the increase in surface area within experimental uncertainty. For the S50 films, the site density measured by the HPLC procedure is lower than the expected value based on surface area, which is presumably due to incomplete access of synthesis reagents to surface sites within the film.

The site density results are further supported by Table 2, which shows the relative hexathymidylate synthesis yield for each of the particle substrates normalized to the yield of the flat glass control (= RSY_{film}/RSY_{flat}). For the 20L and ZL substrates, the yield of full-length 6-mer probes was equal to that of the flat control samples within experimental error, indicating that coupling was equally efficient on these films as on flat glass. On the S50 substrate, synthesis yield was lower and there was a high degree of variability, which is consistent with the data from the site density measurement and indicates that there is poor fluid flow through the small pores in the S50 film during synthesis. Optimization of synthesis (e.g., using higher reagent concentrations and/or longer coupling and washing times) may improve the efficiency of chemical coupling on the S50 substrates but was not pursued further.

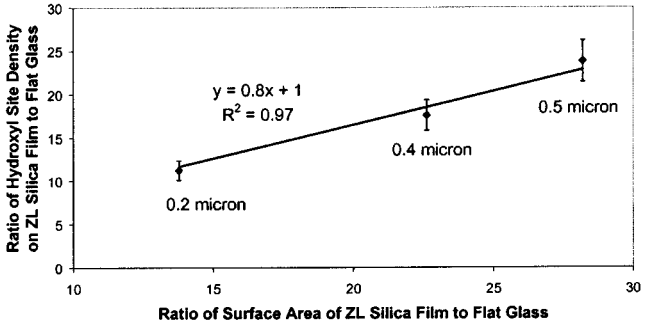

Figure 4. Comparison of the density of accessible hydroxyl sites to the surface area of ZL colloidal silica films of varying thickness. The measured site density increases in direct proportion to the surface area as the film thickness increases.

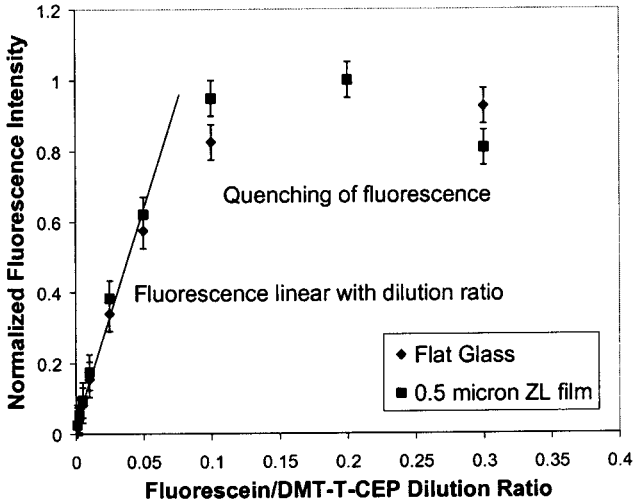

Figure 5. Surface fluorescence on a flat glass surface and a 0.5 μm thick ZL silica film that have been silanated and the hydroxyl sites labeled with fluorescein (see Experimental Section). Fluorescence intensity is in linear proportion to fluorescein/diluent ratio up to a ratio of approximately 0.05; it reaches a maximum at 0.2 and decreases further at higher concentration.

On the basis of these results, the ZL particles were chosen for further experiments. In addition to facilitating efficient coupling, the pores in the ZL films, which are the largest of the three particle types tested, should aid the penetration of large target molecules and fluorescent protein conjugates such as streptavidin−phycoerythrin (SAPE). SAPE is a commonly used labeling agent in GeneChip assays[1] and has dimensions as large as 11 nm.[31] Figure 4 shows that the site density on the ZL films is proportional to the surface area (and the film thickness). For the 0.5 μm film, an increase of 25-fold over flat glass is obtained. Accessibility of surface synthesis sites is independent of film thickness over this range, indicating efficient penetration of synthesis reagents throughout the layer.

Surface Fluorescence. To examine the sensitivity of the system to fluorescence quenching, flat and ZL surfaces were stained with fluorescein in a range of concentrations. Figure 5 shows that the signal on both surfaces is linear with fluorescein/diluent ratio up to 0.05, which corresponds to 1 pmol cm^{-2} of fluorescein.

(31) Glazer, A. N.; Stryer, L. *Methods Enzymol.* **1990**, *184*, 188−194.

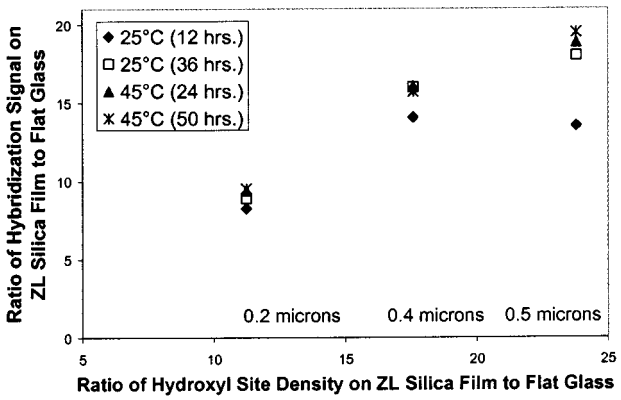

Figure 6. Ratio of binding of oligonucleotide targets (to perfect-match surface-bound probe sequences) on ZL colloidal silica films to fused silica glass. Samples were incubated in 100 nM oligonucleotide target at 25 °C and then at 45 °C. All time points have reached equilibrium within 12 h at 25 °C, except for the 0.4 and 0.5 μm surfaces.

Quenching effects become noticeable at a ratio of 0.1, the signal reaches a maximum at 0.2, and the signal decreases on both films at higher concentrations. On the basis of results from Forman et al.[29] with a similar system, the maximum density of bound fluorophore for 20-mer probes at 25 °C should be approximately 1 pmol cm^{-2}, which is in the linear range for both surfaces.

Optical Scattering. A single front-side "print" with the porous layer in contact with the photolithographic mask was used to determine if the multiple silica/air interfaces in the layer cause significant scattering of light during photolithographic patterning or fluorescent scanning. This is a close mimic of the actual procedures used for manufacturing GeneChip arrays. Colloidal silica layers 0.5, 1, and 2 μm thick were deposited by successive spin-coating depositions and stained with fluorescein dye.[17] For all the coatings tested, the transition "edge" between the background (nonphotolyzed) and stained (photolyzed) regions was as sharp as flat glass. The 20−30 nm pore size is sufficiently smaller than the wavelength of light such that optical scattering does not cause loss of edge resolution during photolithographic synthesis or optical scanning.

Hybridization to Oligonucleotide Targets. Prior to hybridization experiments, the confocal microscope system was calibrated with solutions of oligonucleotide target to correlate the signal to the density of bound target on the flat substrates.[29] Figure 6 shows the hybridization signal ratio for the perfect-match probes on the 0.2, 0.4, and 0.5 μm ZL films relative to flat glass at successive time points. Forman et al. have shown that oligonucleotide probes on flat substrates reach equilibrium with a 10 nM target solution in approximately 1 h,[29] and therefore the 100 nM target used in this study should cause saturation in equal or less time. The bound target density on flat glass reaches a maximum of 0.8 ± 0.2 pmol cm^{-2} at 25 °C for the perfect-match probes, which agrees well with the measured density for similar arrays by Forman et al. and is in the linear range of fluorescence for both flat and ZL silica films (see Surface Fluorescence).

The 0.4 and 0.5 μm ZL films did not reach equilibrium at the first 25 °C time point, but all films appeared to be at equilibrium at the successive time points, as the ratio of the hybridization signal on the films to the signal on the flat glass does not change with additional hybridization time. To ensure that the target was not depleted, fresh solution was replenished after each scan. Hybridization reactions for gene expression assays are commonly performed at 45 °C for 16−24 h^1, which corresponds to the first 45 °C scan in Figure 6. The final time point at 45 °C was taken to ensure that the films had reached equilibrium. The hybridization signal multiple increases in proportion to the film thickness and reaches ~80% of the multiple of the ratio of the hydroxyl site density to flat glass (from Figure 4).

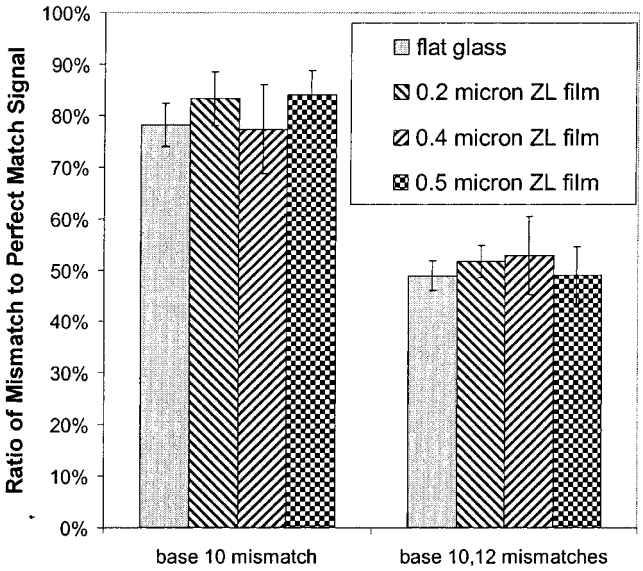

Figure 7. Discrimination ratio on porous glass films after 24 h at 45 °C under saturating conditions (100 nM target). Under these conditions, the discrimination on the porous glass films is equivalent to the flat glass control at each thickness and for both one- and two-base mismatches.

Background and Discrimination. High specificity of discrimination for target molecules as well as low background signals are critical aspects of the functional performance of DNA arrays. Background due to nonspecific adsorption on the silica films was equivalent to flat glass within the uncertainty of the measurement. Background due to the substrate itself increases slightly with film thickness, which may be due to fluorescent impurities in the film. The net result is that at 45 °C, the backgrounds on the 0.2 and 0.5 μm films are 1.4 and 2.1 times the background of the flat glass, respectively. By contrast, bound target reaches multiples of 9 and 19 times the flat glass for the same films, as illustrated in Figure 6.

To test discrimination, probes were synthesized with single-base mismatches at base 10 and two-base mismatches at both base 10 and base 12. Figure 7 shows that discrimination for oligonucleotide targets is equivalent on the flat glass and porous films after 24 h at 45 °C, which is the temperature typically used to destabilize nonspecifically bound targets in gene expression assays. Therefore, the ratio of the hybridization signal on the silica films to flat glass is independent of the binding constant of the probe/target duplex. Since low target densities, such as 0.3 ± 0.1 pmol cm^{-2} at 45 °C for two-base mismatches on the flat glass, and high densities (0.8 ± 0.2 pmol cm^{-2} at 25 °C for the perfect-match probes) are enhanced by the same factor on the

Table 3. Comparison of Measurements on 0.5 μm ZL Films

measurement	(measured ratio to flat glass)/ (surface area ratio to flat glass) (%)
surface area	100
[OH] site density	84 ± 10
surface fluorescence[a]	76 ± 5
hybridization[b]	70 ± 6

[a] Average of measurements with fluorescein/diluent ratios from 0.001 to 0.05. [b] Perfect-match probes.

silica films relative to flat glass, there is further indication that quenching is not more significant on the silica films. If quenching was a factor on the silica films in the concentration range observed, then the multiple at high concentration would be less than the multiple at low concentration, where there is greater distance between fluorophores.

It should be noted that the 100 nM target concentration is much higher than typically present in genomic assays, which typically range from 1 to 100 pM, and was chosen to observe probe/target binding under saturating conditions. A much higher discrimination ratio for the matched and mismatched probes is routinely achieved under practical conditions and hybridization protocols, as discussed by Fidanza et al.,[21] which presents further evidence that discrimination on the colloidal silica films is equivalent to flat glass for gene transcripts of average length approximately 50 bases[1] over a range of concentrations.

Stability. The thickness of the films was tested before and after the hybridization experiments. Within the uncertainty of the measurement, no difference in the thickness of the layer was observed. Additionally, the testing times were much longer than the standard conditions used for gene expression assays.

Discussion

Colloidal silica films created from large colloidal precursors, such as Snowtex 20L and ZL, provide good substrates for high-capacity DNA arrays. Hydroxyl site density on the colloidal silica films is proportional to the surface area, and synthesis yield is equivalent to flat glass. Furthermore, the fact that the probes "function" in the same manner in the porous matrix as on flat glass, as shown by the equivalent discrimination, serves as further evidence that chemical synthesis and hybridization proceed efficiently in the porous matrix. Fluorescence quenching affects both flat and ZL silica films at the same concentration of surface-bound fluorophores, and therefore the signal amplification obtained with the ZL silica films is independent of the bound target concentration over the concentration range examined.

Although both site density and hybridization enhancement on the silica films are proportional to surface area, we observed, by comparison of Figures 4 and 6, that in comparison to flat glass, the enhancement multiple for hybridization < hydroxyl site density < surface area. To understand these results, we must assess the impacts of proximity effects such as steric hindrance and electrostatic repulsion on the performance of the films. The comparison of the multiples obtained from the various techniques provides a starting point to assess these factors, as shown in Table 3. Since the small

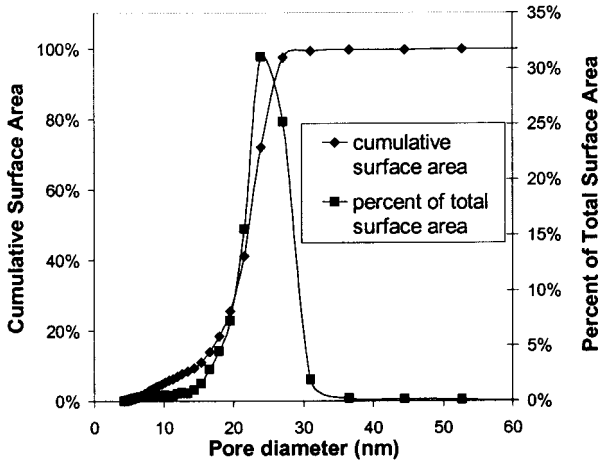

Figure 8. Properties of dried ZL silica solution by nitrogen adsorption. The majority of the area is contained in pores that are ~23 nm in diameter.

nitrogen molecule is used for determination of surface area, this measurement serves as a reference point for the true adsorption capacity of the film. Synthesis and hybridization require the use of larger molecules which may not be able to access all sites on the surface, as will be discussed in the following sections.

Before proceeding with an analysis of proximity effects, it is first necessary to consider the film geometry. Figure 8 shows the incremental and cumulative surface area vs pore diameter for the ZL films, with the pores being the void spaces between the solid particles. The average pore size is 23 nm (see Table 1), and correspondingly the majority of the surface area is in these pores (50% of the surface area is within one standard deviation and 80% is within two standard deviations). Therefore, to further analyze proximity effects, it is necessary to develop a model of the area distribution *within* these pores.

Geometric Model of the Porous System. As is standard in the analysis of porous substrates, a simplified model of a typical pore must be developed, which we have done by consideration of the properties of the porous film. First, the index of refraction of the ZL films is typically 1.3, which corresponds to films that are 68% dense, close to the theoretical packing density for same-sized spheres of 74%.[32] For the ZL suspension, the particle size (D_s) is 65 ± 16 nm and the pore size (D_p) is 23 ± 2 nm. The ratio $D_p/D_s = 0.35$ is similar to the relative size of the octahedral interstitial site in a matrix of close-packed, same-sized spheres, where $D_p/D_s = 0.41$. Therefore, this matrix and interstitial site can serve as a model for the pore geometry, and to obtain a better estimate of the actual spacing in the pore, we have developed a "finite-elements" analysis of the pore space based on this system.

Figure 9a shows a "top view" schematic of the octahedral pore site (with radius = R_p) in a close-packed system of same-sized spheres. To calculate the actual spacing of adjacent surfaces in the pore, we examine a section of sphere S_0, shown as the shaded region. Figure 9b shows that this section, surface ABF, covers $^1/_{16}$th of the surface area of sphere S_0 and is representative of

(32) Kingery, W. D.; Bowen, H. K.; Uhlmann, D. R. *Introduction to Ceramics*, 2nd ed.; Wiley & Sons: New York, 1976; p 57.

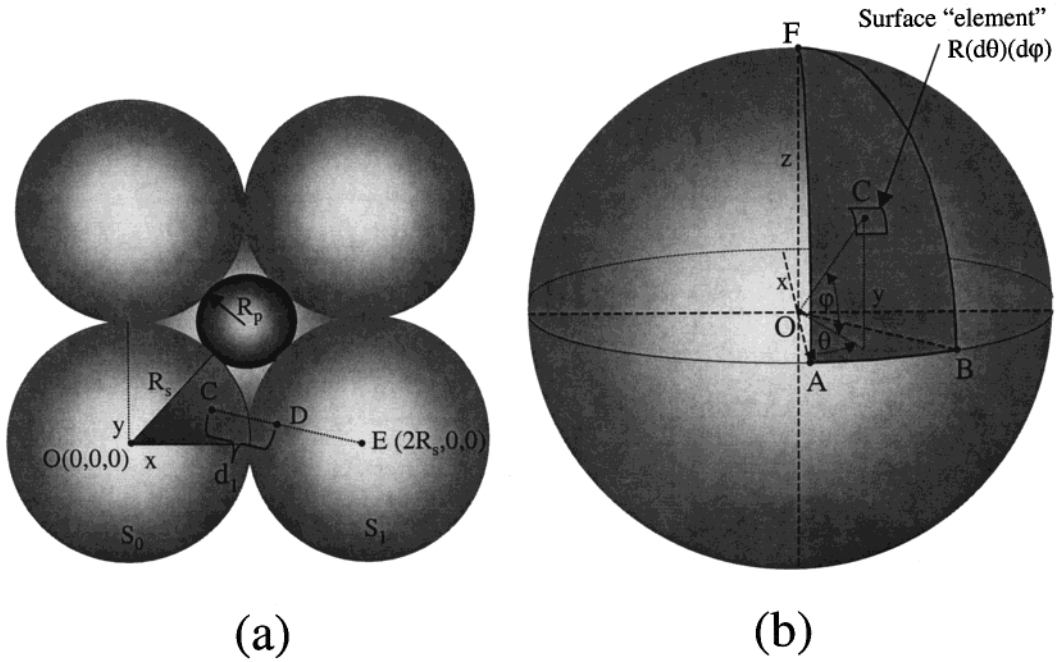

Figure 9. (a) Geometric model of a pore (radius = R_p) between ZL silica particles. The measured pore size (~23 nm) is close to the predicted pore size for the octahedral pore in a close-packed system (~27 nm). (b) For any point C (x_1, y_1, z_1) on surface ABF, d_1 is the shortest distance ("clearance") to point D on an adjacent sphere. The distribution of surface area vs clearance can be determined by calculating the minimum of the distances to sphere S_1 (at {2R, 0, 0}) and S_2 (not shown, "above" pore at {R, R, 1.414R}) for each point on ABF. In the finite-elements approach, each point covers an incremental surface area $R(\mathrm{d}\theta)(\mathrm{d}\varphi)$.

the surface inside the void space. For a given point C (at {x_1, y_1, z_1}) on surface ABF, the distance d_1 to the closest point D on adjacent sphere S_1 can be calculated by drawing a line from C to the origin of sphere S_1 (point E). As a line extending from the radius is perpendicular to the tangent at that point, the segment CD is the shortest distance to the adjacent particle. The same calculation can be done for sphere S_2 (not shown, "above" pore at {R, R, 1.414R}). Equations 3a−3f have been used to determine the distance distribution.

$$x = R\cos\varphi\cos\theta \tag{3a}$$

$$y = R\cos\varphi\sin\theta \tag{3b}$$

$$z = R\sin\varphi \tag{3c}$$

$$d_1 = R(\sqrt{(x_1 - 2)^2 + y_1^2 + z_1^2} - 1) \tag{3d}$$

$$d_2 = R(\sqrt{(x_1 - 1)^2 + (y_1 - 1)^2 + (z_1 - \sqrt{2})^2} - 1) \tag{3e}$$

$$d = \min(d_1, d_2) \tag{3f}$$

d is defined as the "clearance" or the shortest distance to a point on an adjacent particle. θ and φ are shown in Figure 9b. Surface ABF is divided into elements with surface area $R(\mathrm{d}\theta)(\mathrm{d}\varphi)$, and the closest point to an adjacent particle for each element is determined. By increasing θ from 0 to 45° and φ from 0 to 90°, we can determine the distribution of surface area vs clearance, as shown in Figure 10. It is evident from the figure that the actual distances between points on adjacent surfaces is much less than implied by the "average" pore size distribution. This distribution provides the context for assessing the factors in Table 3.

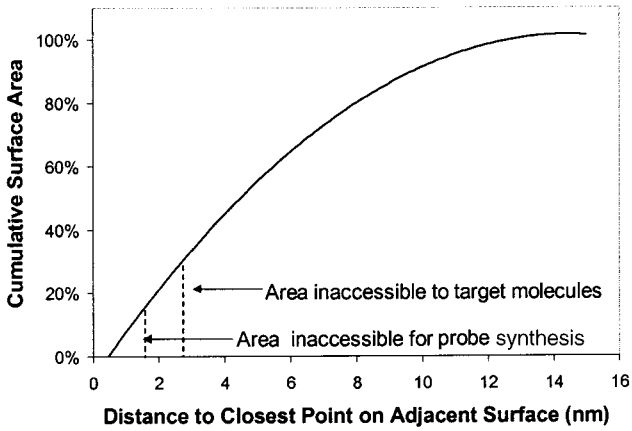

Figure 10. Distribution of surface area within 23 nm pores. Points on the surface of a given particle are much closer to a point on an adjacent surface than implied by the "average" pore size. The silane layer, which is 1−2 nm thick, causes ~15% of the surface, located in the crevices of the large pores, to be inaccessible for probe synthesis. During hybridization, target molecules are not able to access probe sites in the crevices, excluding an additional 15% of the surface.

Site Density and Coupling Yield. Prior to coupling of oligonucleotide probes, the surface is coated with a silane coating, the thickness of which has been determined to be 1−2 nm.[33] The density of sites measured by the HPLC C_3-fluorescein procedure was 84% of the surface area increase (see Table 3). On the basis of Figure 10, this result implies that the effect of the silane layer is to occlude from probe synthesis approximately the first 1.5 nm of clearance, which agrees well with the measured thickness of the silane.

(33) Forman, J., unpublished data. Silane thickness measured by atomic force microscopy "scratch test" using Digital Instruments nanoscope.

Surface Fluorescence. Figure 5 shows that neither the flat surface nor the porous films are susceptible to quenching at surface concentrations below approximately 1 pmol cm^{-2}, which is greater than the measured density of adsorbed target for the assays in this study. Although the measured surface fluorescence increase is slightly lower than the available hydroxyl site density increase, the two measurements agree within experimental uncertainty (see Table 3), and quenching effects within the pores will not be considered further.

Hybridization to Oligonucleotide Targets. Two cases of proximity effects, such as steric and electrostatic repulsion, are possible: (1) effects due to lateral spacing of probes on the surface of a particle and (2) effects due to clearance between adjacent particles.

Proximity Effects Due to Lateral Spacing of Probes. On the basis of the good agreement between the surface area of the films and the density of hydroxyl sites, it can be assumed that the lateral spacing between probes (and therefore between adsorbed target molecules) on the silica particles is approximately the same as their spacing on a flat surface. The closest spacing of adjacent target molecules is estimated by assuming a rectangular array of sites (eq 4), where σ is the density of bound target (mol cm^{-2}) and N_A is Avogadro's number.

$$s = \frac{1}{(\sigma N_A)^{1/2}} = \frac{1}{((1 \times 10^{-12})(6.02 \times 10^{23}))^{1/2}} = 1.29 \times 10^{-6}\ \text{cm} = 12.9\ \text{nm} \quad (4)$$

For double-stranded DNA, $L = Nb_o$, where L is the length of the duplex, N the number of bases, and b_o is 3.4 Å.[34,35] For a 20-mer duplex, $L = 6.8$ nm, which represents the maximum distance from the attachment to the surface that the duplex can extend, and therefore probe/target duplexes should not exert significant steric or electrostatic influences on neighboring duplexes.

Proximity Effects Due to Clearance. The extended duplex could be long enough to span small pores and crevices in large pores. As shown in Figure 8, small pores of 10 nm and less comprise only ~5% of the surface area in the film. It is evident that these small pores do not impede the penetration of the target or that the target is able to find alternative routes, as the amount of bound target increases in proportion to the film thickness (see Figure 6). The influence of the smallest pores on hybridization kinetics has not been evaluated, and it may prove that proximity effects in the small openings have a profound effect on the hybridization rate.

Proximity effects within the crevices of the large pores were also considered. Two cases are possible: (1) initial target penetrates the crevice, forms probe/target duplex, and prevents penetration of further target or (2) target never penetrates the crevice. For case 1, hindrance could be possible from a minimum length of the duplex width (~2 nm for double-stranded DNA in solution[34]) to a maximum of the duplex length (6.8 nm). On the basis of Figure 10 and assuming that the first 1.5 nm of clearance is excluded by the presence of the silane coating, we find that these hindrances would block up to ~40 and ~80% of the sites, respectively. Therefore, based on the data in Table 3, where it is cited that bound target reaches ~70% of the available surface area, we conclude that the limiting factor is the duplex width rather than the length.

For case 2, sites spaced more closely than the radius of gyration of the diffusing molecule would be inaccessible. For a single-stranded target molecule diffusing in solution, the radius of gyration R_g of the random coil can be estimated from eq 5.[35]

$$R_g = (Lp/3)^{1/2} \quad (5)$$

$L = Nb_o$, and for single-stranded DNA, b_o has been calculated as 4.3 Å.[35] p is the persistence length, which approaches the intrinsic persistence length p_i for single-stranded DNA of 8−13 Å for the high ionic strength solutions used in this study.[35] With the use of $p = 13$ Å and $N = 20$, R_g was estimated at a maximum of 19 Å. This length is similar to the width of the duplex, so it is difficult to assess which is the ultimate cause of limitation, and further studies with targets of much different probe lengths would be necessary. Additionally, long targets may be able to temporarily "unwind" from the random coil formation they take in free solution and diffuse through openings smaller than the radius of gyration. Fidanza et al.[20] reports that the ability to uniquely identify target sequences was not affected when fragmented biological targets with average length of approximately 50 bases[1] were hybridized to the porous matrix. In summary, the amount of bound target on the porous layers approaches the maximum possible for this type of surface morphology, given the fundamental limitations of the duplex width and the size of the diffusing target molecules.

Conclusion

A porous inorganic system has been characterized and evaluated for use with small molecule assays such as DNA arrays. Oligonucleotide synthesis and DNA hybridization have been carried out in pore sizes on the order of the length of a probe/target duplex. The porous films show equivalent performance to flat glass in terms of efficiency of chemical coupling, resolution of photolithographic patterning, optical scanning, and discrimination for target molecules but yield greatly increased hybridization signals. Hybridization signals reach ~70% of the maximum possible intensity based on the surface area of the porous films, and we have presented a model that attributes the 30% hindrance to the portion of the film that is inaccessible to synthesis reagents and/or target molecules.

Colloidal silica substrates take longer to reach saturation than flat glass. Films that are 0.2 μm thick reached equilibrium with the target solution in less than 12 h at room temperature, whereas thicker films (0.4 and 0.5 μm) reached equilibrium in 12−36 h. The difference in time constants is most likely due to a combination of limitations, including that mass transfer from solution may not be rapid enough to meet the increased demand for target of the high-capacity surface and that the diffusivity of the target may be reduced

(34) Stryer, L. *Biochemistry*, 4th ed.; W. H. Freeman and Company: New York, 1998; p 791.
(35) Tinland, B.; Pluen, A.; Sturm, J.; Weill, G. *Macromolecules* **1997**, *30*, 5763−5765.

in the porous matrix. Aspects of the hybridization behavior such as kinetics and diffusion are currently being investigated in greater depth.

In comparison to other techniques for creating high-density surfaces for biomolecule array applications, colloidal silica films offer several advantages. For example, the use of silica as the base material makes these films easy to integrate into array-fabrication processes on glass or oxidized metal surfaces. Additionally, since DNA probes on the particle films thermodynamically behave the same as on flat glass, much of the knowledge gained from the extensive research conducted on standard flat glass substrates can be readily translated to these films, without the necessity of considering other types of target/matrix interactions that could occur with other matrix materials. These properties make colloidal silica substrates promising candidates for future use in high-capacity DNA arrays.

Acknowledgment. We acknowledge the assistance and support of Larry Bailey, John Bravman, Alice Gast, Albert Lee, Fabian Pease, and Lubert Stryer of Stanford University. We also thank Paul Bury, Paul Ciccolella, Steve Fodor, Jon Forman, Bill Lyon, Dan Mutnick, Nineveh Parker, Michael Savage, Audrey Suseno, and Mark Trulson of Affymetrix. Richard Vinci of Lehigh University was extremely helpful with advice and technical assistance, and Mike Alden of Beckman−Coulter assisted with nitrogen adsorption measurements.

CM010578N